Hyperfine Interact (2016) 237: 50
DOI 10.1007/s10751-016-1290-9

Structural and Mössbauer studies of nanocrystalline Mn^{4+}-doped $Li_{0.5}Fe_{2.5}O_4$ particles prepared by mechanical milling

H. M. Widatallah[1] · F. N. Al-Mabsali[1] · F. S. Al-Hajri[1] · N. O. Khalifa[2] · A. M. Gismelseed[1] · A. D. Al-Rawas[1] · M. Elzain[1] · A. Yousif[1]

Published online: 22 February 2016

Abstract The structure and magnetic properties of spinel-related Mn^{4+}-doped $Li_{0.5}Fe_{2.5}O_4$ nanocrystalline particles of the composition $Li_{0.5}Fe_{2.25}Mn_{0.1875}O_4$, prepared by milling a pristine sample for different times, were investigated. The average crystallite and particle size, respectively, decreased form ∼40 nm to ∼10 nm and ∼2.5 μm to ∼10 nm with increasing milling time from 0 h to 70 h. Rietveld refinement of the XRD data of the non-milled sample show the Mn^{4+} dopant ions to substitute for Fe^{3+} at the octahedral B-sites of the spinel-related structure. The Mössbauer spectra of the milled ferrites indicate that more particles turn superparamagnetic with increasing milling time. The Mössbauer data collected at 78 K suggest that while in the non-milled sample the Mn^{4+} ions substitute for Fe^{3+} at the octahedral B-sites, this is reversed as milling proceeds with doped Mn^{4+} ions, balancing Fe^{3+} vacancies and possibly Li^+ ions progressively migrate to the tetrahedral A-sites. This is supported by the slight increase observed in the magnetization of the milled samples relative to that of the non-milled one. The magnetic data suggest that in addition to the increasing superparamagentic component of the milled particles, thermal spin reversal and/or spin canting effects are possible at the surface layers of the nanoparticles.

Keywords Lithium ferrites · Defects · Nanoparticles · Mössbauer spectroscopy · XRD

This article is part of the Topical Collection on *Proceedings of the International Conference on the Applications of the Mössbauer Effect (ICAME 2015), Hamburg, Germany, 13-18 September 2015*

✉ H. M. Widatallah
hishammw@squ.edu.om

[1] Physics Department, College of Science, Sultan Qaboos University, PO Box 36, Muscat 123, Oman

[2] Physics Department, Faculty of Science, University of Khartoum, PO Box 321, Khartoum 11115, Sudan

1 Introduction

The spinel lithium ferrite, $Li_{0.5}Fe_{2.5}O_4$, adopts an inverse spinel structure in which all the Li^+ ions and three-fifths of all Fe^{3+} ions occupy octahedral B-sites, whilst the remaining Fe^{3+} ions occupy tetrahedral A-sites in the O^{2-} fcc lattice [1–4]. At low temperatures, the structure is indexed with the space group is $P4_332$ with the cations of the octahedral sub-lattice arranged in ordered fashion, whereas at temperatures above 735–755 °C, the occupancy of the octahedral sites becomes disordered and the material is indexed to the space group $Fd\bar{3}m$ [3, 4]. The material is of interest due to its technologically attractive electric and magnetic properties that render it useful in, for example, microwave and memory-core applications [1–4]. These properties depend on the super-exchange ionic interactions J_{AB}, J_{AA} and J_{BB}, and are thus determined by the type and distribution of the constituent cations over both crystallographic sites. The introduction of ionic substitutes for Fe^{3+} into either site can, therefore, lead to modified physical properties that may suit novel applications [1–5]. Alternatively reducing the particle size to the nanometre scale [6, 7] can result in properties that are different from those of the corresponding pure and cation-substituted lithium ferrite. Presumably this is due to the structure of the nanoparticle which may be modelled as a bulk-isostructural core and a large volume fraction cation-disordered surface (shell) layer [7]. Indeed the possibility of producing ferrite particles ranging in size from the micrometre scale all the way down to a few nanometres is technologically attractive as it offers a means of tailoring size-dependent properties that may be technologically desirable [6–9].

Among the various processing methods used to prepare inorganic nanoparticles, mechanical milling has become increasingly popular due to its relative ease, flexibility and low-cost. Previously we have reported on the evolution of structural magnetic properties of Mg^{2+}-doped $Li_{0.5}Fe_{2.5}O_4$ as a function of particle size when the material was milled for different times and related that to the distribution of the cations and defects (substitutional and interstitial impurities) over both crystallographic sites at the shells and cores of the nanoparticles [7]. We also have used atomistic interatomic potential calculations to show that the presence of the divalent Mg^{2+}ions requires excess Li^+ impurity ions to stabilize the spinel structure [10]. Such a defect structure is obviously different from that expected when tetravalent Mn^{4+} ions substitute for trivalent Fe^{3+} ones in $Li_{0.5}Fe_{2.5}O_4$ as Fe^{3+} vacancies and/or impurity Fe^{2+} ions (due to the reduction of Fe^{3+}) are required for charge neutrality. Hence it is of interest to see how the distribution of cations and point defects evolves as the size of Mn^{4+}-doped $Li_{0.5}Fe_{2.5}O_4$ particles is reduced to the nanometre scale and how this affects their magnetic properties. In this article we report on combining x-ray diffraction (XRD) and Mössbauer spectroscopy to investigate the structure of nanocrystalline Mn^{4+}-doped $Li_{0.5}Fe_{2.5}O_4$ particles, whose sizes are reduced by subjecting a pristine sample to milling for different times, and correlate that with their observed magnetic properties.

2 Experimental

In Mn^{4+}-doped $Li_{0.5}Fe_{2.5}O_4$, where the Fe^{3+} ions are substituted with Mn^{4+} ones, charge balance leads to a compositional formula of the form $Li_{0.5}Fe_{2.5-x}Mn_yO_4$ where $y = 3x/4$. Accordingly for $x = 0.25$, Mn^{4+}-doped $Li_{0.5}Fe_{2.5}O_4$ the composition $Li_{0.5}Fe_{2.25}Mn_{0.1875}O_4$ was prepared using the conventional ceramic method starting from a 0.25: 1.25: 0.1875 molar mixture of Li_2CO_3, α-Fe_2O_3, and MnO_2. The mixture was manually ground, compressed into pellets, heated in air in a Carobllite (HTF 1800) furnace at

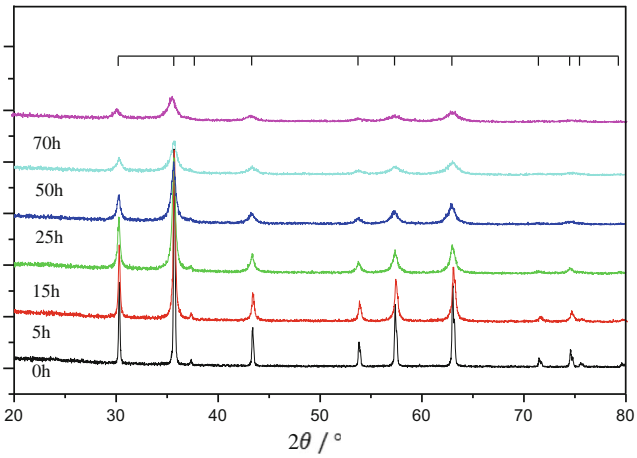

Fig. 1 The XRD patterns of the $Li_{0.5}Fe_{2.25}Mn_{0.1875}O_4$ milled for the times shown. The vertical axis is the intensity (arb. units)

1000 °C (h) and slowly cooled in the furnace. The product was milled for different times in air using a Fritch D-55743 P6 milling machine with tungsten carbide vial and balls. The balls-to-mass ratio was 17:1, the milling speed was 200 rpm and the. XRD patterns were collected using a PANalytical X'Pert PRO X-ray diffractometer using Cu$-k\alpha$radiation ($\lambda =$ 1.5406Å). The program MAUD was used for Rietveld structural refinement of XRD data [11]. The particle size and morphology were studied using a JEOL (JEM 2100F) transmission electron microscope (TEM) operating at a voltage of 200 kV. ^{57}Fe Mössbauer spectroscopic measurements were performed at 300 K and 78 K using a 50 mCi ^{57}Co/Rh source in the transmission geometry and the spectrometer was operating in the constant acceleration mode. The Mössbauer chemical isomer shifts are quoted relative to α-Fe at 298 K. Spectra were fitted with the program Recoil [12] assuming lorentzian line shape for all absorption sites. A vibrating sample magnetometer (DMS-1660 VSM) was used for magnetic measurements.

3 Results and discussion

The XRD patterns recorded from the $Li_{0.5}Fe_{2.25}Mn_{0.1875}O_4$ samples milled for 0 h, 5 h, 15 h, 25 h, 50 h and 70 h are shown in Fig. 1. For the non-milled sample, the XRD pattern is characterized by sharp reflection peaks that index to a single inverse-spinel phase (space group: $Fd3m$). For the other samples, the spinel structure is clearly preserved throughout the milling process with the reflection peaks progressively broaden and decrease in intensity. This implies an increasing structural disorder as the crystallite size reduces with increasing milling time that leads to different inter-atomic distances at the nanoparticles' surface layers relative to those at their cores. The resultant distribution of lattice parameters leads to the observed broadening of the reflection peaks. Rietveld refinement of the XRD pattern of the non-milled sample (Fig. 2 and Table 1) showed the best fit to the experimental data to be obtained with all doped Mn^{4+} ions exclusively substituting for 75 % of the expelled Fe^{3+} ions at the octahedral B-sites.

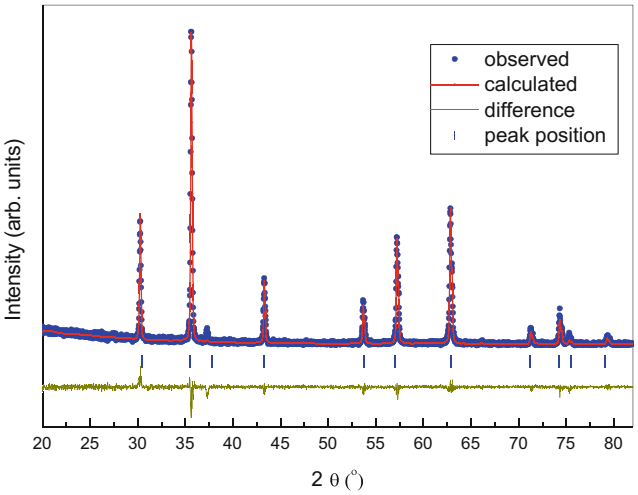

Fig. 2 Observed, calculated and difference XRD patterns of the non-milled $Li_{0.5}Fe_{2.25}Mn_{0.1875}O_4$ nanocrystalline particles. The bars refer to the position of Bragg's reflection peaks of the indicated phases

Table 1 Refined structural positions of the cations/anions in the non-milled $Li_{0.5}Fe_{2.25}Mn_{0.1875}O_4$ sample.

Ion	Wyckoff's position	x/a	y/b	z/c	Occ.
$Li+$	16d	0.6250	0.6250	0.6260	0.25000
Fe^{3+}	16d	0.6250	0.6250	0.6250	0.62500
Mn^{4+}	16d	0.6250	0.6250	0.6250	0.09375
Fe^{3+}	8a	0.0000	0.0000	0.0000	1.00000
O^{2-}	32e	0.3849	0.3849	0.3849	1.00000

It is pertinent to recall that in ref. [7] we have shown that the XRD patterns Mg^{2+}-doped $Li_{0.5}Fe_{2.5}O_4$ nanocrystalline particles, prepared using a similar route, exhibit reflection peak-broadening that depended on *(hkl)* rather than on the scattering angle. In that case the best Rietveld fits to the XRD patterns were attained assuming two spinel-related phases rather than one. The bulk-like phase was assigned to the nanoparticles' cores whereas the distorted phase with cationic positions and distributions that are slightly different from those of the bulk was assigned to their surface layers (shells). The XRD patterns of the present Mn^{4+}-doped $Li_{0.5}Fe_{2.5}O_4$ nanocrystalline particles (Fig. 1), however, do not exhibit sufficiently tangible asymmetric peak-broadening to perform similar Rietveld refinements to distinguish between the nanoparticles' cores and shells as was done for the Mg^{2+}-doped $Li_{0.5}Fe_{2.5}O_4$ nanocrystalline particles [7]. Hence, we only deduced average features such as the average crystallite size which decreased from ∼40 nm to ∼10 nm when the milling time varied between 0 h and 70 h as is shown in Fig. 3. No significant variation of the lattice parameter relative to that of the non-milled sample (8.3639 Å) was found to be induced by milling [2–4].

The TEM micrographs of the non-milled $Li_{0.5}Fe_{2.25}Mn_{0.1875}O_4$ particles and those obtained after milling for 70 h, depicted in Fig. 4, illustrate how milling affected the particle morphology and size. While the non-milled sample is composed mostly of large particles,

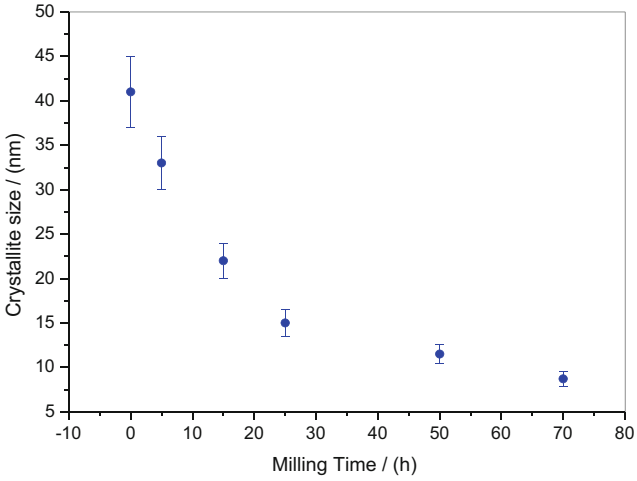

Fig. 3 Crystallite size as a function of the milling time for the milled nanocrystalline particles of $Li_{0.5}Fe_{2.25}Mn_{0.1875}O_4$

including some cubic single crystals, with an average size of $\sim$ 2.5 μm the sample milled for 70 h is composed of agglomerates of irregularly shaped nanoparticles with an average size of $\sim$10 nm.

The 298 K and 78K ^{57}Fe Mössbauer spectra collected from all milled $Li_{0.5}Fe_{2.25}Mn_{0.1875}O_4$ samples are presented in Figs. 5 and 6, respectively. The corresponding fitted Mössbauer parameters are given, respectively, in Tables 2 and 3.

For the non-milled sample each spectrum is well fitted with two magnetic sextets due to Fe^{3+} at the tetrahedral and octahedral A- and B- sites. The outer sextet with the larger isomer shift and hyperfine magnetic field was assigned to the B-site [2, 4–7]. The isomer shift values (δ) at both sites, which are typical of Fe^{3+} in high spin state, are consistent with those expected for spinel lithium ferrite [2, 4, 6, 7]. The difference between the isomer shift values of both sextets at both temperatures is significantly smaller than that of pure $Li_{0.5}Fe_{2.5}O_4$ ($\Delta\delta$ $\sim$0.21 mm/s) [7] and is indicative of covalency effects due to the insertion of the Mn^{4+} substitution. The absence of any Fe^{2+} spectral component confirms that no reduction of Fe^{3+} to Fe^{2+} has taken place to balance the presence of Mn^{4+} in the ferrite structure. The quadrupole shift (Δ) values for both sextets (almost zero) indicate that the incorporation of Mn^{4+} ions in the inverse spinel structure leads to no deviation from cubic symmetry at both sub-lattices [2, 4, 6, 7]. The fact the magnetic hyperfine fields (H_{eff}) for both sites are slightly less than the corresponding values for the pure $Li_{0.5}Fe_{2.5}O_4$ [2, 7] indicates a weakening in the magnetic fields at both sites and could be ascribed to the substitution of Mn^{4+} (3 μ_B) for Fe^{3+} (5 μ_B). This together with the Fe^{3+} vacancies at the B-site, as indicated by the XRD Rietveld analysis above, weaken the Fe_A–O–Fe_B exchange interaction and consequently lead to the observed smaller hyperfine fields [5–7].

It has been shown by Dormann et al [5] that the relative Fe^{3+} ion occupation of the A- and B-sub-lattices in $Li_{0.5}Fe_{2.5}O_4$ obtained from a zero-field Mössbauer spectrum recorded at 78 K is similar to that obtained from an in-field (6.5 T) spectrum recorded at 4.2 K. This, in turn, implies the 78 K Mössbauer recoilless fractions at the A- and B-sites in $Li_{0.5}Fe_{2.5}O_4$, f_A and f_B respectively, may be assumed to be almost similar [5]. If we further assume that

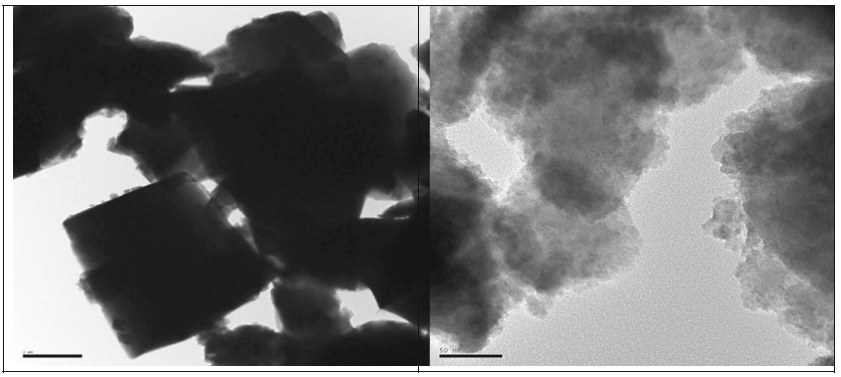

Fig. 4 The TEM micrographs of the $Li_{0.5}Fe_{2.25}Mn_{0.1875}O_4$ particles milled for (*left*) 0 h and (*right*) 70 h. The scale bar for the *left* micrographs represents 1 μm and for the *right* micrograph represents 50 nm

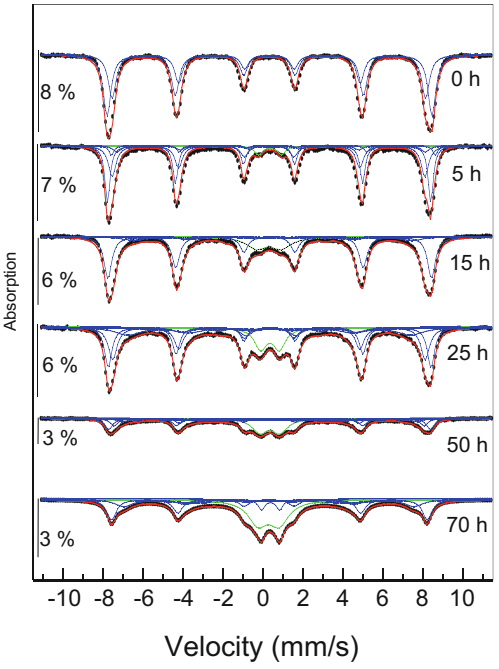

Fig. 5 The 298 K ^{57}Fe Mössabuer spectrum recorded from the $Li_{0.5}Fe_{2.25}Mn_{0.1875}O_4$

these recoilless fractions are not affected upon doping with Mn^{4+} ions, then the decrease at 78 K in the relative spectral area of the B- site sextet (55%) for the non-milled Mn^{4+}-substituted $Li_{0.5}Fe_{2.5}O_4$ relative to (60%) for pure $Li_{0.5}Fe_{2.5}O_4$ is consistent with the XRD result that the Mn^{4+} ions substitute for Fe^{3+} ones at octahedral B-sites.

We now turn to the 298 K Mössbauer spectra of the milled $Li_{0.5}Fe_{2.25}Mn_{0.1875}O_4$ nanocrystalline particles (Fig. 5; Tables 2). Each spectrum is composed of a magnetic sex-line pattern superimposed on a central doublet whose area steadily increases with milling time. The Mössbauer absorption lines clearly broaden as the milling time increases revealing a growing disorder of the Fe^{3+} cationic distribution at both A- and B-sites. In spinel

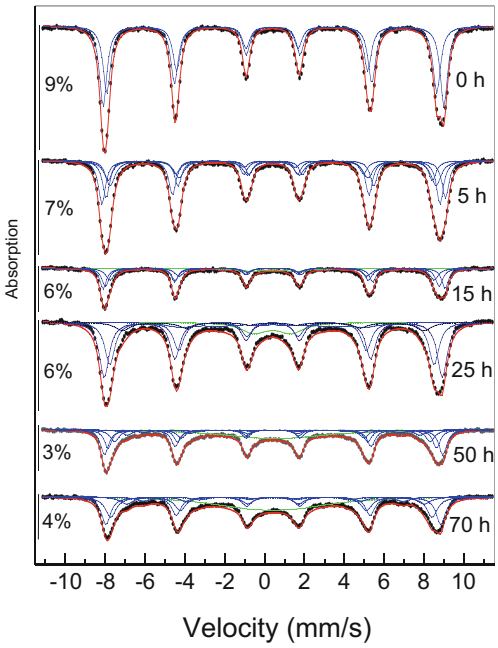

Fig. 6 The 78 K ^{57}Fe Mössabuer spectrum recorded from the $Li_{0.5}Fe_{2.25}Mn_{0.1875}O_4$

ferrites, owing to the supertransferred mechanism, the Fe^{3+} nuclei at either sites are sensitive to any change in the number of their nearest other-site magnetic neighbors and this sensitivity was shown to be more pronounced for the B-site Fe^{3+} ions [5, 13]. Hence a broad distribution of magnetic hyperfine fields, particularly for the B-site, may be expected due to the milling induced changes in cation distribution. Accordingly multiple sextets are required to fit the Mössbauer spectra of the milled $Li_{0.5}Fe_{2.25}Mn_{0.1875}O_4$ nanocrystalline particles. The sextets labeled A and B, whose isomer and quadrupole shifts (Δ) are almost similar to those of the non-milled $Li_{0.5}Fe_{2.25}Mn_{0.1875}O_4$ samples, but with reduced hyperfine magnetic fields, are assumed respectively to be due to Fe^{3+} ions at the A- and B- sites in the milled sample. The reduction in the magnetic hyperfine fields with increasing milling time could be related to weakening of the super-exchange interaction at the surface ions due to bond weakening. Such a surface effect should also result in asymmetric line shapes [7], but obviously an asymmetry of this kind is expected to be less pronounced in the spectra as the particle size gets smaller. This suggests that in addition to the surface effect, the hyperfine field decreases due to a size effect which could be associated with collective excitations where the magnetization is thermally excited to oscillate in the direction of minimum energy resulting to a particle-size-dependent hyperfine fields that are smaller than those of the corresponding bulk [14]. This is possibly the reason why for the samples milled for 50 h and 70 h, the best fits of the Mössbauer spectra required using the an additional sextet (M), with very small hyperfine fields, which we assign to very small particles with volumes slightly bigger than the blocking volume where the ferrite particles turn superparamagnetic. Evidently here we only refer to the average hyperfine field of the Fe^{3+} at both sites. The central doublet required for fitting the 298 K spectrum (Fig. 5 and Table 2) is mainly attributed to superparamagnetic particles as its area is significantly reduced in the spectra recorded at 78 K (Fig. 6 and Table 3).

Table 2 298 K ^{57}Fe Mössbauer parameters for the $Li_{0.5}Fe_{2.25}Mn_{0.1875}O_4$ particles milled for the times shown

Time (h)	Sub-spectrum	δ(±0.02 mm/s)	Δ (±0.002 mm/s)	H_{eff} (±0.02 T)	Area (±1%)
0	A	0.29	−0.014	48.65	42
	B	0.31	0.004	50.41	58
5	A	0.26	−0.008	44.77	37
	B(1)	0.32	0.003	50.38	48
	B(2)	0.39	0.058	45.55	6
	B(3)	0.42	0.027	48.43	6
	D	0.26	1.450		3
15	A (1)	0.29	−0.007	48.53	36
	B(1)	0.47	−0.166	26.68	3
	B (2)	0.32	0.006	50.21	39
	B (3)	0.44	0.030	43.20	10
	D	0.28	1.250		12
25	A (1)	0.30	−0.008	48.50	28
	A (2)	0.29	−0.012	27.12	8
	B (1)	0.32	0.004	50.08	28
	B (2)	0.33	−0.037	43.88	19
	D (1)	0.39	2.483		5
	D (2)	0.34	0.937		13
50	A (1)	0.30	−0.003	48.09	14
	B (1)	0.36	0.009	41.65	6
	B (2)	0.32	0.002	49.91	22
	B (3)	0.33	−0.002	45.71	9
	M	0.50	0.004	20.03	24
	D (1)	0.33	0.999		25
70	A\	0.29	−0.015	44.98	19
	B	0.31	0.002	49.00	29
	M	0.34	0.003	23.73	14
	D (2)	0.37	0.902		5
	D (3)	0.27	1.070		33

Each of the 78 K Mössbauer spectra of the milled $Li_{0.5}Fe_{2.25}Mn_{0.1875}O_4$ nanocrystalline particles (Fig. 6 and Table 3) is composed of a broadened six-line pattern superimposed on a very weak central doublet, which could be due to particles still undergoing superparamagnetic relaxation with blocking temperatures of less than 78 K. Again the magnetic spectra were fitted using sextets due to Fe^{3+} at the A- and B-sites with the hyperfine parameters summarized in Table 3. The isomer shift values for both types of sextets are larger than those obtained at 298K due to the second order Doppler shift [8] while their almost zero quadrupole shifts (Δ) reflect a nearly cubic symmetry. Using the argument that the 78 K Mössbauer spectra allow for accurate determination of the cation distribution, and concentrating on the 78 K spectral areas of the Fe^{3+} ions at both crystallographic sites in the larger (magnetic) particles, it is interesting to see how milling progressively induces an Fe^{3+} cationic migration from the tetrahedral A-site to the octahedral B-site. The A-site to B-site

Table 3 78 K ^{57}Fe Mössbauer parameters for the $Li_{0.5}Fe_{2.25}Mn_{0.1875}O_4$ particles milled for the times shown

Time (h)	Sub-spectrum	δ (±0.02 mm/s)	Δ (±0.002 mm/s)	H_{eff} (±0.02T)	Area (±1%)	A : B (magnetic)
0	A	0.37	−0.009	51.25	45	45 :55
	B	0.44	0.010	52.91	55	
5	A	0.36	0.003	50.54	39	41:59
	B(1)	0.41	0.027	52.89	48	
	B(2)	0.500	−0.095	51.74	8	
	D	0.50	2.640		5	
15	A	0.37	0.015	51.83	32	35:65
	B (1)	0.48	0.012	53.10	34	
	B (2)	0.40	−0.024	50.33	25	
	D	0.46	2.220		9	
25	A	0.38	−0.015	50.36	31	34:66
	B (1)	0.41	−0.010	28.56	10	
	B (2)	0.42	0.011	52.48	39	
	B (3)	0.43	0.003	46.74	10	
	D	0.393	1.860		10	
50	A (1)	0.38	0.003	50.46	31	36: 64
	A (2)	0. 33	0.170	29.46	4	
	B (1)	0.44	0.015	52.43	25	
	B (2)	0.47	0.011	45.54	25	
	D	0.49	2.014		15	
70	A(1)	0.39	−0.046	49.90	18	26: 74
	B(1)	0.44	0.003	51.98	22	
	B (2)	0.49	0.057	46.17	7	
	B(3)	0.46	−0.024	40.32	5	
	B(4)	0.48	0.003	22.69	18	
	D	0.37	2.24		30	

Fe^{3+} relative population ratios obtained decreases from 45 : 55 for the non-milled sample to 26: 74 for the sample milled for 70 h. This could only be possible if the doped Mn^{4+}, the balancing Fe^{3+} vacancies and possibly some Li^+ ions progressively migrate from the octahedral B-site to the tetrahedral A-sites as milling proceeds. This is indicative of how increasingly disordered the shells layers of the nanoparticles become. Such a cationic distribution should increase the magnetization as the milling time increases. To confirm this we show in Fig. 7 variation of the magnetization M of the milled $Li_{0.5}Fe_{2.25}Mn_{0.1875}O_4$ particles milled for 15 h, 50 h and 70 has a function of the applied magnetic field measured at 298K. All the cycles present a hysteretic behavior characteristic of soft materials. It is clear that, in consistency with the cationic distribution derived from the 78 K Mössbauer data, the magnetization at the maximum increases with increasing milling time. However, no such an effect is observed for the almost zero coercivity and remanent magnetization that appear to be unaffected by the reduction of the particle size due to milling. The fact that the measured magnetization is much less than the theoretically expected one using the Néel's collinear model [2, 7] is partly due to the increasing superparamgentic nature of these particles at

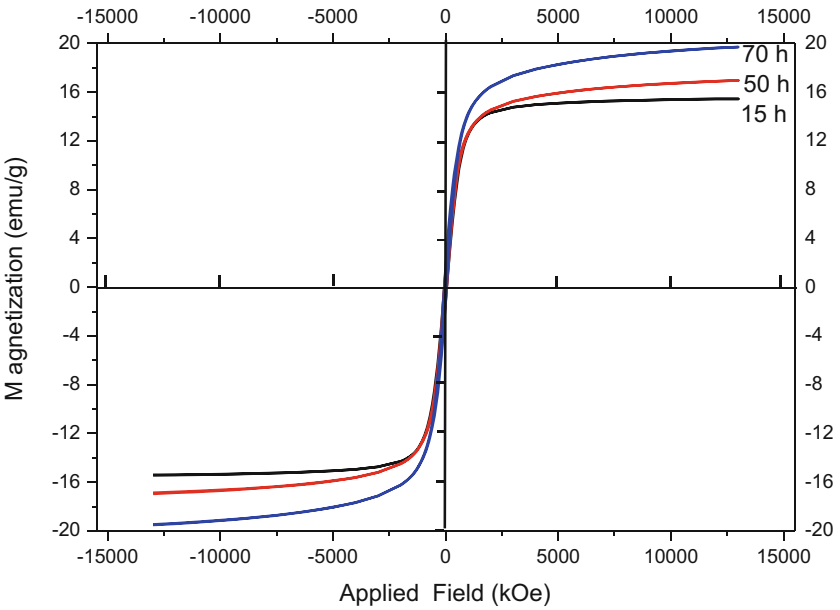

Fig. 7 Magnetization (M) versus applied magnetic field cycles at 298K of the and after milling for the times shown

higher milling times and also to thermal spin reversal and/or spin canting effects that may take place the surface layers of the nanoparticles.

Acknowledgment This work is supported by a Sultan Qaboos University research grant (IG/SCI/PHYS/14/04. HMW acknowledges the continuous support of Intisar Sirour.

References

1. Baba, P.D., Argentina, G.M.: IEEE Tarns. Microwave Theory Technol. **22**, 654 (1974)
2. Widatallah, H.M., Johnson, C., Berry, F.J., Pekala, M.: Solid State Commun. **120**, 171 (2001)
3. Widatallah, H.M., Moore, E.A.: J. Phys. Chem. Solids **65**, 1663 (2004)
4. Widatallah, H.M., Johnson, C., Berry, F.J., Gismelseed, A.M., Jartych, E., Marco, J.F., Gard, F.S., Pekala, M.: J. Phys. Chem. Solids **67**, 1817 (2006)
5. Dormann, J.L., Tomas, A., Nogues, M.: Phys. Status Solidi a **77**, 611 (1983)
6. Widatallah, H.M., Berry, F.J.: J. Solid State Chem. **164**, 230 (2002)
7. Widatallah, H.M., Johnson, C., Gismelseed, A.M., Al-Omari, I.A., Stewart, S.J., Al-Harthi, S.H., Thomas, S., Sitepu, H.: J. Phys. D: Appl. Phys. **41**, 165006 (2008)
8. Sepelak, V., Tkacova, K., Boldyrev, V.V., Wibmann, S., Becker, K.D.: Physica B **234–236**, 617 (1997)
9. Jiang, J.Z., Goya, G.F., Rechenberg, H.R.: J. Phys. Condens. Matter **11**, 4063 (1999)
10. Widatallah, H.M., Moore, E.A., Babo, A.A., Al-Barwani, M.S., Elzain, M.: Mater. Res. Bull. **47**, 3995 (2012)
11. Lutterotti, L., Matthies, S., Wenk, H.-R.: Int. Union Crystallogr. Newslett. **21**, 14 (1999)
12. Lagarec, K., Rancourt, D.G.: Nucl. Instrum. Methods **129**, 266 (1998)
13. Yang, H., Wang, Z., Zhao, M., Wang, J., Han, D., Lou, H., Wang: Mater. Chem. Phys. **48**, 60 (1997)
14. Mørup, S., Topsøe, H.: Appl. Phys. **11**, 63 (1976)